Wave-Function Engineering of CdSe/CdS Core/Shell Quantum Dots for Enhanced Electron Transfer to a TiO2 Substrate

ARTICLE *in* THE JOURNAL OF PHYSICAL CHEMISTRY C · AUGUST 2010

Impact Factor: 4.77 · DOI: 10.1021/jp102978g

7 AUTHORS, INCLUDING:

Zhijun Ning
ShanghaiTech University
58 PUBLICATIONS **2,726** CITATIONS
SEE PROFILE

Haining Tian
Uppsala University
46 PUBLICATIONS **2,359** CITATIONS
SEE PROFILE

Hans Agren
KTH Royal Institute of Technology
867 PUBLICATIONS **18,561** CITATIONS
SEE PROFILE

Wave-Function Engineering of CdSe/CdS Core/Shell Quantum Dots for Enhanced Electron Transfer to a TiO_2 Substrate

Zhijun Ning,*,† Haining Tian,‡ Haiyan Qin,† Qiong Zhang,† Hans Ågren,† Licheng Sun,‡ and Ying Fu*,†

Department of Theoretical Chemistry, School of Biotechnology, Royal Institute of Technology, SE-106 91 Stockholm, Sweden, and Department of Chemistry, School of Chemical Science and Engineering, Royal Institute of Technology, Teknikringen 30, 10044 Stockholm, Sweden

Received: April 2, 2010; Revised Manuscript Received: August 5, 2010

In this paper, we have synthesized a series of core/shell quantum dots (QDs) for the purpose of enhancing the electron transfer from the dots to a TiO_2 substrate. We make use of the fact that CdSe is a small-bandgap material compared with CdS; therefore, in a common CdSe/CdS core/shell QD, the photo-excited electron is confined deeply in the CdSe core. By special construction of the CdS/CdSe core/shell QDs, referred as reversed type-I, the electron wave function will distribute largely in the shell region. This facilitates the transfer of the electron from the QD to the TiO_2 substrate, resulting in significantly improved electron-injection efficiency. Such an enhanced electron-injection efficiency was confirmed by fluorescence lifetime decay measurements, showing the largest lifetime reduction after that the QDs were adsorbed on the TiO_2 surface. The reversed type-I CdS/CdSe QDs show a much higher photon-to-current conversion efficiency than type-I CdSe/CdS and CdSe QDs without shell. Furthermore, by chemical-bath depositing of CdS on the QD-sensitized electrode to form a quantum-well structure, the electron recombination between the QDs and the redox couple was reduced, hence further enhancing the electron-injection efficiency. The absorbed-photon-to-current efficiency of the quantum well CdS/CdSe/CdS sensitized solar cells reaches a value as high as 60%.

1. Introduction

Colloidal semiconductor nanocrystals have been the subject of great scientific and technological efforts, with promising potential applications including biological tagging materials,[1,2] photovoltaics,[3,4] and display devices.[5] In particular, colloidal-nanocrystals-based solar cells have in recent time triggered interest for their potential superiority over traditional inorganic semiconductors or organic dye sensitizers. This owes to the fact that, compared with traditional semiconductor cells, colloidal nanocrystals share all of the primary advantages of organics-scalable and controlled synthesis and the ability to be processed in solution.[3] Furthermore, compared with organic dyes, inorganic colloidal nanocrystals are more stable under harsh environments, and narrow-bandgap nanocrystals are more efficient for harvesting long-wavelength solar irradiation. Various kinds of photovoltaic devices based on inorganic nanocrystals, such as CdS,[6] CdSe,[7] PbS,[8] InAs,[9] Bi_2S_3,[10] and CdTe,[11] have been developed, for example, metal-junction solar cells,[12] polymer hybrid solar cells,[13] and quantum dot-sensitized solar cells (QDSCs).[14] However, the efficiency of these cells is significantly lower than that of traditional organic solar cells[15] or inorganic heterojunction solar cells.[16] Two critical factors that restrict the efficiency are their relatively low electron-injection efficiency and large electron-recombination rate.[17] Generally speaking, the electrons and holes are expected to be quantum-confined within the inner part of the nanoparticles, which intrinsically restricts the electron injection.[18] Various configurations of nanocrystals, such as nanorods or hyperbranched semiconductor nanocrystals, have been developed to improve the electron-injection efficiency of nanocrystal-based solar cells.[19] For QDSCs, Kamat et al. observed that the electron-injection efficiency at the excitonic band increased with the decrease of the size of the quantum dots (QDs), which was ascribed to the increase of the driving force by the uplift of the conduction band of QDs.[7a] Recently, Pal et al. found that electron-transport dynamic from CdSe/ZnS core/shell QDs to benzoquinone or TiO_2 depends upon the size of the CdSe core.[20] The ball-like QD configuration tends to enhance the quantum-confinement effect, which makes it more difficult to extract electrons. Although colloidal QDs can expose special multiexciton-generation (MEG) character,[21] the efficiencies based on colloid QDs are usually low. Recently, it was found that MEG electrons moved so slowly that they recombined largely with holes and lost their energy before the electrode TiO_2 could snag them.[21c,d] Therefore, in order to improve the performance of solar cells based on QDs and to utilize the MEG effect, it is critical to improve the electron-injection efficiency.

Although electrons and holes are normally confined in the central part of the spherical QDs, we envisage that the photogenerated electrons can more easily be extracted if they can be engineered to distribute on the external part of the QD. Therefore, we construct in this work a core/shell QD structure by using barrier material as the core and using the well material as the shell in order to confine the photogenerated electrons in the shell.[22] By adsorbing this kind of colloidal QDs on the TiO_2 surface, we expect to obtain an increased electron-injection rate when compared with the simple core QDs. In addition, by the chemical-bath deposition (CBD), a layer of semiconductor material with higher energy level can be adsorbed on the colloidal QDs which are already adsorbed on the TiO_2 to form quantum wells.[23] By restricting the photoelectrons in the middle

* Corresponding author. E-mail: ningzj82@theochem.kth.se, fyg@theochem.kth.se.
† School of Biotechnology.
‡ School of Chemical Science and Engineering.

10.1021/jp102978g
Published on Web 08/19/2010

wells and keeping the contact between the quantum well and the TiO_2 substrate, the electron-injection efficiency will be further enhanced.

2. Experimental Methods

Recently, Peng et al. developed a novel synthesis method for the shell growth of core/shell-type QDs by successive ion layer adsorption and reaction (SILAR) on the cores QDs.[24] In this way, the shell system was nearly precisely controlled, homogeneous, and epitaxial. Therefore, we synthesized the reversed type-I CdS/CdSe QDs by the SILAR method and compared its performance with single-component CdSe QDs in QDSCs. For comparison, we also synthesized type-I CdSe/CdS QDs, where the conduction band of the CdS shell is higher than the CdSe core. The synthesis detail is listed in the Supporting Information.

The QDs-sensitized TiO_2 electrode was prepared according to the procedure reported in the literature.[7a] TiO_2 colloidal dispersion was made according to ref 25 by employing commercial TiO_2 (P25, Degussa AG, Germany). Films of nanocrystalline TiO_2 colloidal on Fluoride-doped tin oxide (FTO) were prepared by sliding a glass rod over the conductive side of the FTO. Sintering was carried out at 450 °C for 30 min. The thickness of the TiO_2 film was about 8 μm. The TiO_2 electrodes were immersed in a 1 mol/L (M) mercaptopropionic-acid-acetonitrile solution for 12 h and then transferred to the QDs toluene solution. The electrodes were left in the solution for two days to ensure saturated adsorption of the QDs onto the TiO_2 electrodes. The growth of CdS by the CBD process resembles the procedure described in ref 6c. The photoanode was dipped into a methanol solution containing $Cd(NO_3)_2$ (0.2 M) for 4 min, rinsed with methanol, then dipped for another 4 min into a Na_2S methanol solution (0.2 M), and rinsed again with methanol. The two-step dipping procedure is termed as one CBD cycle. The adsorbed amount of CdS can be increased by repeating the assembly cycles, and five cycles were carried out for each colloidal QDs samples. The QD-modified TiO_2 electrode and a Pt-coated counter electrode were juncted by using 30 μm thick thermoplastic film (TPS 065093, Dyesol). The electrolyte solution consists of Na_2S (0.5 M), S (0.125 M), and KCl (0.2 M) in water/methanol (7:3 by volume) solution.[6c] IPCE measurements were carried out with a Xenon arc lamp (300 W), a 1/8 m monochromator, a source/meter, and a power meter with a 818-UV detector head. For each kind of QDs, five cells were prepared and tested. The IPCE fluctuation for the same kind of QDs is within 5%, and the one with the medium value was chosen as the final data.

3. Results and Discussion

The absorption spectra of CdSe QDs in toluene are shown in Figure 1. **CdSe-1** and **CdSe-2** exhibit the first absorbance peak at 515 and 564 nm, respectively. On the basis of the Peng's empirical equation,[26] the corresponding radii of **CdSe-1** and **CdSe-2** are calculated to be 1.3 and 1.7, nm respectively. To further confirm the size of QDs, high-resolution transmission electron microscopy (HRTEM) was used (Figure 2). The HRTEM image and size distribution figure of **CdSe-2** is shown in Figure S1 in the Supporting Information. The average diameter of **CdSe-2** is measured to be about 3.4 nm, which agrees well with Peng's empirical data. The HRTEM images of **CdSe/CdS-1** and **CdSe/CdS-2** are shown in Figure S1 in the Supporting Information and Figure 2, respectively. The average diameters of **CdSe/CdS-1** and **CdSe/CdS-2** are 4.4 and 5.7 nm, respectively. Because the thickness for one layer of CdS is 0.37 nm, for **CdSe/CdS-1** and **CdSe/CdS-2**, about 1.5 and 2.5 layers of CdS shells were coated on the CdSe core, respectively.[27] The absorption spectra of the CdSe/CdS core/shell QDs in toluene are shown in Figure 1 as well. The first absorbance peak of **CdSe/CdS-1** and **CdSe/CdS-2** are 578 and 590 nm, respectively. The fluorescence apex for **CdSe/CdS-1** and **CdSe/CdS-2** are 603 and 615 nm, respectively.

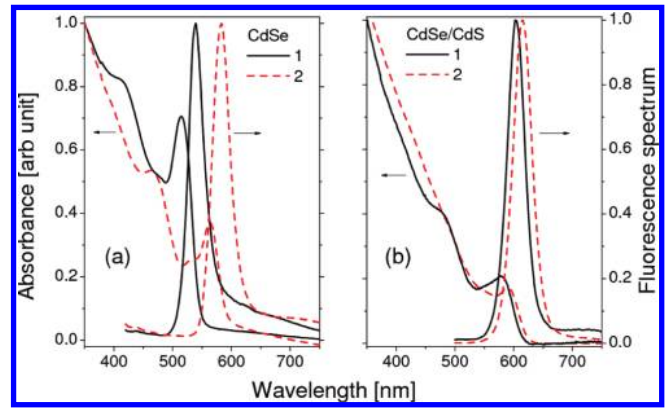

Figure 1. Absorption and fluorescence spectra of CdSe (a) and CdSe/CdS (b) QDs. Two QDs are presented in each QD type: solid lines represent **CdSe-1** (a) and **CdSe/CdS-1** (b) and dash lines represent **CdSe-2** (a) and **CdSe/CdS-2** (b).

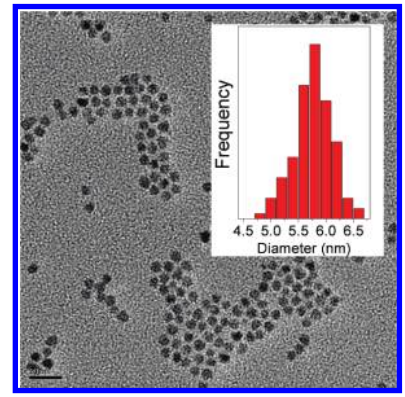

Figure 2. The HRTEM image of **CdSe/CdS-2**; scale bar equals 20 nm.

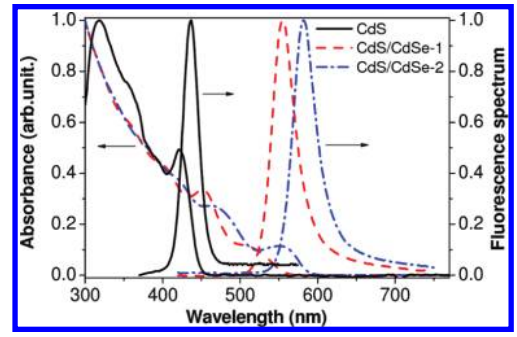

Figure 3. Absorbance and fluorescence spectra of CdS and CdS/CdSe QDs. Solid lines represent CdS, dash lines represent **CdS/CdSe-1**, and dot lines represent **CdS/CdSe-2**.

The absorbance and fluorescence spectra of the CdS core QDs in toluene are shown in Figure 3. The first absorbance peak is 421 nm (Table 1). By empirical equations,[26] the corresponding QD radius is obtained to be about 2.0 nm. The half bandwidth of the fluorescence apex is just 25 nm, indicating a narrow size distribution. The absorbance and fluorescence spectra of the CdS/CdSe core/shell QDs are shown in Figure 3 as well. It can be seen that, with the increase of the shell thickness, the

TABLE 1: Geometric Structures and Optical Characteristics of Core-Shell QDs

QDs	core r_1 [nm]		total radius r_2 [nm]		absorbance [nm]		fluorescence [nm]
	empirical-data fitting	band-structure calculation	empirical-data fitting	band-structure calculation	exp.	band-structure calculation	
CdS	2.0	1.9			421	430	437
CdS/CdSe-1	2.0	1.9	2.9	2.9	510	513	555
CdS/CdSe-2	2.0	1.9	3.3	3.5	549	559	582
CdSe-1	1.3	1.5			515	516	539
CdSe-2	1.7	1.7			564	560	582
CdSe/CdS-1	1.6	1.7	2.1	2.2	578	565	603
CdSe/CdS-2	1.6	1.7	2.5	2.6	590	584	615

absorbance and fluorescence spectra of **CdS/CdSe-2** were both bathochromically shifted. The fluorescence maximum for **CdS/CdSe-1** and **CdS/CdSe-2** are 555 and 582 nm, respectively. Because the average thickness of a monolayer of CdSe is about 0.36 nm, the calculated average QDs radii of **CdS/CdSe-1** and **CdS/CdSe-2** are about 2.9 and 3.3 nm, respectively.[24]

Table 1 lists geometric structures and wavelengths of the lowest-energy absorbance peak and fluorescence peak. The radii of the cores and the core−shells in the empirical-data-fitting columns are obtained by empirical-data fitting of ref 26 by using the measured absorbance- and fluorescence-peak wavelengths as well as by comparing with refs 24 and 27, and the values listed in the band-structure-calculation columns are calculated by effective medium theory.[2] By referring to the vacuum level as potential energy zero, the conduction band (CB) edge of CdSe is −4.95 eV (electron affinity of CdSe), the band gap (energy difference between CB and valence band, i.e., VB) is 1.74 eV, and the quantum-confinement energy for the valence-band hole is 1.5 eV.[28] The electron affinity of CdS is 4.5 eV, and the bandgap is 2.42 eV.[29] The wave-function distributions of ground-state electrons in these core/shell QDs are shown in Figure 4. For CdSe/CdS QDs, the coating of CdS shell does not modify the electron distribution, because the corresponding ground state is already largely confined in the CdSe core region (with a CdSe core radius of 1.7 nm under investigation). In the CdS/CdSe QD, the conduction bandedge in the CdSe shell is lower than in the CdS core, and the ground-state energy level is also determined by the thickness of the shell. When the CdSe shell is thin, size effect dominates; therefore, the ground state is largely distributed in the CdS core region. By coating the CdS core with a CdSe shell and increasing the CdSe shell thickness, we eventually redistribute the wave function of the ground electron state from the CdS core region to the CdSe shell, as demonstrated in Figure 4b. We thus can expect an enhanced electron-injection efficiency.

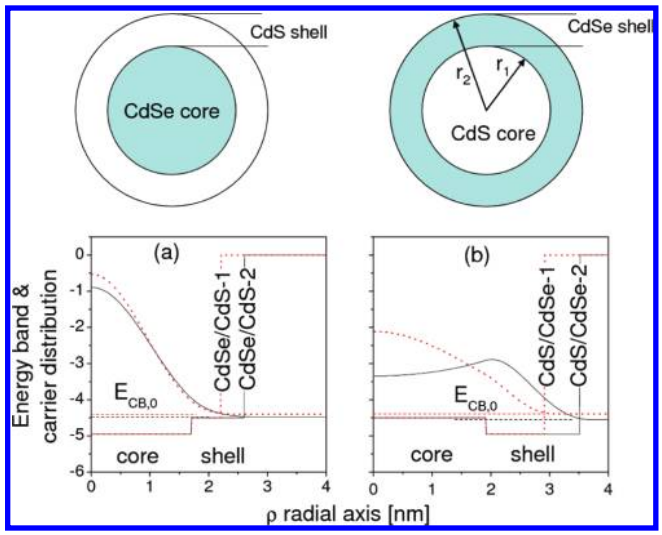

Figure 4. Ground-state ($E_{CB,0}$, horizontal dashed line) of electron in the conduction band and its wave-function distribution in the core/shell CdSe/CdS (a) and CdS/CdSe (b) QDs. Two QDs are presented in each QD type: the black solid line represents thick shell (**CdSe/CdS-2**: $r_1 = 1.7$ nm, $r_2 = 2.6$ nm; **CdS/CdSe-2**: $r_1 = 1.9$ nm, $r_2 = 3.5$ nm), and the red dotted line represents the thin shell (**CdSe/CdS-1**, r2 $r_2 = 2.2$ nm; **CdS/CdSe-1**, $r_2 = 2.6$ nm).

The absorption and fluorescence change spectra of **CdS/CdSe-2** on TiO_2 film as the CBD growth of CdS are shown in Figure 5. It can be seen that the absorbance increased mainly in the CdS absorption region of 400−500 nm, whereas in the long wavelength region, where the CdSe part mainly contributes, the increase was observable but weak. The absorption and fluorescence spectra are slightly bathochromically shifted, indicating the growth of CdS on the CdS/CdSe-QD-adsorbed TiO_2 film. The small fluorescence peak between 500−550 nm originates most probably from a few CdS nanocrystals directly grown on TiO_2 during the CBD process. Figure 6 shows the absorption spectra of **CdSe-2**, **CdSe/CdS-2**, and **CdS/CdSe-2** adsorbed on the TiO_2 without (left) and with (right) five cycles of CBD growth of CdS. **CdSe-2** shows the largest bathochromical shift due to the CBD process. The absorption spectra of **CdSe-1**, **CdSeS-1**, and **CdS/CdSe-1** on the TiO_2 film have a change trend similar to that of the CdS growth, which are shown in the Supporting Information.

We further analyzed the excited QDs deactivation by monitoring the fluorescence decay. Figure 7 shows the fluorescence decay of **CdSe/CdS-2** and **CdS/CdSe-2**. The fluorescence lifetime decay spectra of **CdSe-2, CdSe/CdS-1**, **CdSe-1**, and **CdS/CdSe-1** are shown in the Supporting Information. Triexponential decay kinetics was found to be satisfactory in the determination of the fluorescence lifetimes. These values were then used to estimate the average lifetime of the QD fluorescence decay by using the expression below:[7a]

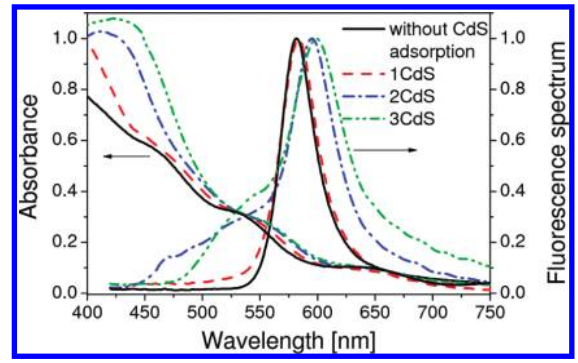

Figure 5. Absorbance and fluorescence change spectra of **CdS/CdSe-2** on TiO_2 without (solid lines) and with the CBD growth of one (1CdS, dash lines), two (2CdS, dash-dot lines), and three (3CdS, dash-dot-dot lines) cycles of CdS.

$$\langle\tau\rangle = \frac{B_1\tau_1^2 + B_2\tau_2^2 + B_3\tau_3^2}{B_1\tau_1 + B_2\tau_2 + B_3\tau_3} \quad (1)$$

The calculated lifetime values of the QDs are listed in Table 2. When comparing with QDs on glass, the fluorescence decay lifetime significantly decreased when adsorbed on TiO_2. The lifetime decrease was attributed to the electron transfer to TiO_2, the rate constant (K_{et}) of which can be calculated by the equation below:[7a]

$$K_{et} = \frac{1}{\tau_{(QD+TiO_2)}} - \frac{1}{\tau_{(QD)}} \quad (2)$$

where $\tau_{(QD+TiO_2)}$ represents the fluorescence lifetime of QDs on TiO_2 film and $\tau_{(QD)}$ is the fluorescence lifetime of QDs on glass. By using the lifetimes listed in Table 2, we get electron-injection constants of 0.0813, 0.2013, and 0.3575 ns^{-1} for **CdSe/CdS-2**, **CdSe-2**, and **CdS/CdSe-2**, respectively.[7a] The electron-injection constant of **CdS/CdSe-2** is distinctly larger than those of **CdSe/CdS-2** and **CdSe-2**. This observation confirms that the reversed type-I CdS/CdSe QDs are favorable for the electron injection. **CdS/CdSe-2** QDs with thicker CdS shells show faster electron-injection constants than **CdS/CdSe-1** with thinner shells. It is actually expected by the theoretical energy band structure in Section 3 that the wave function of the electron ground state is more confined in the external thick shell, thereby facilitating the electron injection from the QDs to the TiO_2 contact and reducing the radiative recombination. For the normal type-I CdSe/CdS QDs, the electrons are concentrated in the core part, which is undesirable for the electron transfer from the QDs to TiO_2 and results in slower electron injection. Furthermore, as can be seen in the electron-distribution simulation in Figure 4, the increase of the CdS shell thickness leads to a larger distance from the electron concentrated center to the surface of the QDs, a phenomenon that explains the smaller electron-injection constant of **CdSe/CdS-2** compared with that of **CdSe/CdS-1**. It can thus be concluded that the wave-function distribution in the QDs is important for the electron injection. A fast electron injection is expected to facilitate the solar-energy conversion, which is also confirmed by the following device characterization.

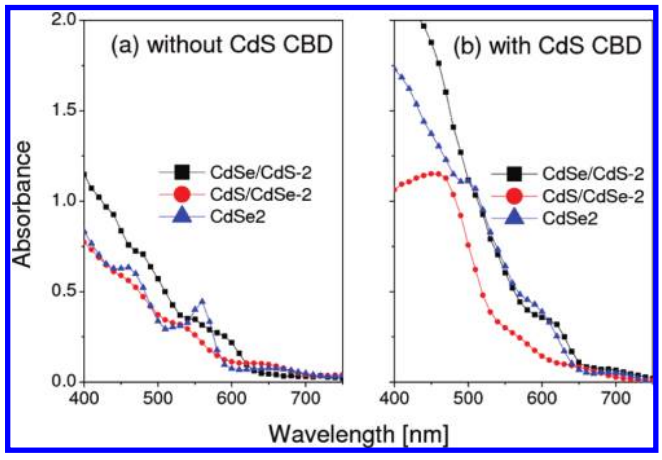

Figure 6. Absorption spectra of **CdSe/CdS-2**, **CdS/CdSe-2**, and **CdSe-2** on the TiO_2 photoanode without (a) and with (b) the growth of CdS.

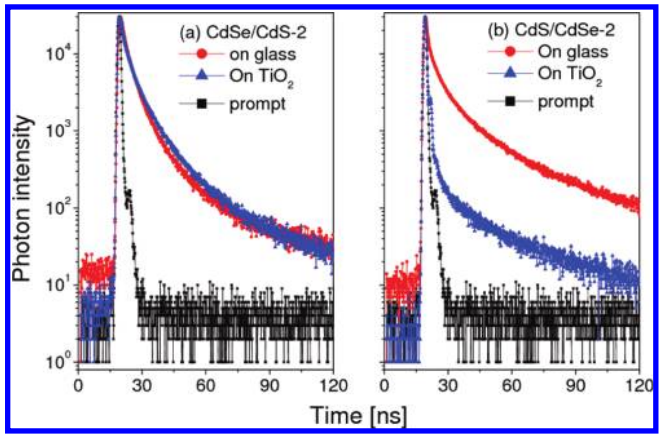

Figure 7. Time-resolved fluorescence transient spectra of **CdSe/CdS-2** (a) and **CdS/CdSe-2** (b) on glass and TiO_2.

The energy-conversion efficiency of QDs sensitized solar cells to monochromatic light irradiation was analyzed in terms of incident-photon-to-current efficiency (IPCE).[10] The IPCE action spectra for **CdSe-2**, **CdS/CdSe-2**, and **CdSe/CdS-2** sensitized solar cells are presented in Figure 8. The IPCE spectra closely match the absorption spectra of the QDs adsorbed on the TiO_2 film. The observations confirm that the photocurrent generation in the QDSCs originates from the QDs. The IPCE action spectra for **CdS/CdSe-1** and **CdSe/CdS-1** sensitized solar cells are shown in Supporting Information (Figure S3). Like the increase of the shell thickness, the photoresponse region is bathochromically shifted as well, indicating that the energy-conversion spectra can be tuned by varying the size of the core/shell QDs. The highest IPCE values for **CdSe-2**, **CdSe/CdS-2**, and **CdS/CdSe-2** are 17.5, 11.3, and 25.2%, respectively, which are consistent with their electron-injection constants.

The IPCE can also be expressed by the following equation[30]

$$\mathrm{IPCE}(\lambda) = [1 - 10^{-\mathrm{Abs}(\lambda)}]\phi_{inj}\eta_c \quad (3)$$

where $\mathrm{Abs}(\lambda)$ is the absorbance of the photoanode at wavelength λ, ϕ_{inj} is the electron-injection efficiency, and η_c is the efficiency of collecting the injected electrons at the back contact. The product of ϕ_{inj} and η_c is the absorbed-photon-to-current efficiency (APCE). Therefore, the APCE can be calculated from the following equation:[30]

$$\mathrm{APCE}(\lambda) = \mathrm{IPCE}(\lambda)/[1 - 10^{-\mathrm{Abs}(\lambda)}] \quad (4)$$

When considering the similar configuration of all these QDSCs, the efficiency of collecting the injected electrons at the back contact (η_c) could be analogous.[30] Thus, the change of electron-injection efficiency (ϕ_{ext}) could be the main factor that affects the APCE values. When considering the differences in the absorption capability of these QDs on TiO_2, which have not been calculated in the IPCE, it seems better to use the APCE values in the comparison of electron-injection efficiencies. On the basis the IPCE spectra and absorption spectra on TiO_2, the APCE spectra of **CdSe/CdS-2** and **CdS/CdSe-2** were calculated; the results are shown in Figure 9. The APCE spectra of other QDs are shown in the Supporting Information (Figure S4). The highest APCE values for the **CdSe-2**, **CdSe/CdS-2**, and **CdS/CdSe-2** QDs are 24.2, 12.3, and 33.4%, respectively. **CdS/CdSe-2** shows a much higher APCE than **CdSe/CdS-2** and **CdSe-2**, which is in agreement with the tendency in electron-injection constant. Meanwhile, in line with the electron distribution in the QDs (Figure 4), the APCE of **CdS/CdSe-2** is distinctly higher than that of **CdS/CdSe-1**, which further confirms that localizing the electron in the external part of the

TABLE 2: Fluorescence Lifetime Data of the Studied QDs

	T_1 (ns)	T_2 (ns)	T_3 (ns)	B_1	B_2	B_3	CHISQ	$\bar{T}$ (ns)	K_{et} (±0.03) (ns^{-1})
CdSe/CdS-1	8.43	2.29	35.99	0.039	0.065	0.0040	1.52	13.34	0.11
CdSe/CdS-1-TiO_2	4.65	23.12	0.78	0.030	0.0023	0.25	1.60	9.74	
CdSe/CdS-2	6.52	33.79	0.84	0.034	0.0059	0.14	2.27	15.54	0.081
CdSe/CdS-2-TiO_2	1.13	5.50	19.38	0.093	0.042	0.0038	1.87	6.87	
CdS/CdSe-1	3.59	38.58	0.37	0.0077	0.0014	0.50	1.71	8.68	0.31
CdS/CdSe-1-TiO_2	1.56	25.56	0.23	0.032	0.00069	0.75	2.28	2.36	
CdS/CdSe-2	5.70	29.05	0.50	0.031	0.0050	0.21	2.58	12.51	0.36
CdS/CdSe-2-TiO2	2.46	0.26	8.24	0.036	0.43	0.0043	2.41	2.29	
CdSe-2	7.66	33.10	1.33	0.047	0.0090	0.15	1.64	15.08	0.20
CdSe-2-TiO2	4.42	19.73	0.30	0.0092	0.0016	0.52	1.49	3.74	

QDs can effectively enhance the electron-injection efficiency. In contrast, electrons in the CdSe/CdS QDs are mainly concentrated at the core part, which results in a much lower electron-injection efficiency. Consistent with the electron-injection constant, the APCE of **CdSe/CdS-2** decreases as the shell thickness increases.

After the CdS's CBD growth on the sensitizer photoanode of colloidal-QD-on-TiO_2, the APCEs of all samples increased dramatically, among which **CdS/CdSe-2** shows the highest APCE of 60.2%, much higher than those of **CdSe/CdS-2** (43.1%) and **CdSe-2** (50.6%). There might be a few CdS QDs grown on the unadsorbed TiO_2 surface directly, which may contribute to the improvement of the electron-injection efficiency in the CdS absorption region. The IPCE spectrum of cells with sole adsorption of CdS by CBD process is shown in Figure S5 in the Supporting Information. To compare more precisely the change of electron-injection efficiency of the colloidal QDs after the CBD growth of CdS, we compared the APCE values above 540 nm where there is no obvious contribution from the independent CBD CdS growth (Figure S6 in the Supporting Information). The APCE of **CdS/CdSe-2** at 540 nm increased from 7.7 to 31.2%, whereas that of **CdSe/CdS-2** increased from 7.8 to 21.0%. It was suggested that the CBD adsorption increased the coverage of QDs on TiO_2 surface, which reduced the charge recombination between TiO_2 and redox couple, resulting in a greatly increased photon-to-current conversion efficiency.[6h,7d] The much more increased APCE of **CdS/CdSe-2** is most probably caused by the reduced electron recombination between QDs and redox couple. Because the electrons in **CdS/CdSe-2** are concentrated on the shell part, they are more susceptible to the electron recombination between the QDs and the redox couple in the electrolyte. However, after the CdS growth, **CdS/CdSe-2** formed the quantum-well structure, which effectively reduced the electron recombination and further enhanced the electron-injection efficiency. The photocurrent-versus-time curves are shown in Figure S8 in the Supporting Information. For **CdSe-2**, **CdS/CdSe-2**, and **CdSe/CdS-2** QDs-based QDSCs, the photocurrents are stable for at least 30 min under simulated AM 1.5 (100 mW/cm^2) irradiation.

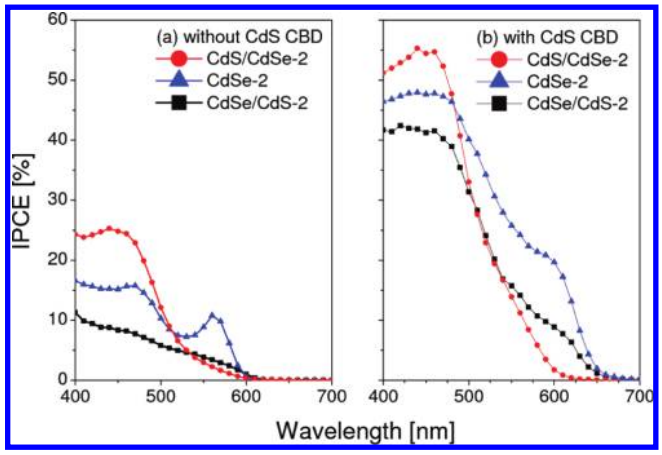

Figure 8. IPCE spectra of **CdSe/CdS-2**, **CdS/CdSe-2**, and **CdSe-2** QDs sensitized solar cells without (a) and with (b) the growth of CdS.

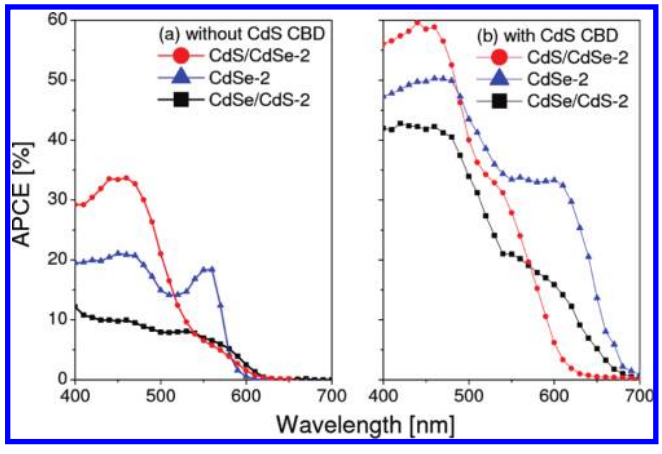

Figure 9. APCE spectra of **CdSe/CdS-2**, **CdS/CdSe-2**, and **CdSe-2** QDs sensitized solar cells without (a) and with (b) the growth of CdS.

4. Conclusion

In conclusion, we have studied the electron transfer between a series of core/shell QDs, synthesized at our laboratory, and a TiO_2 substrate. The idea was to construct CdS/CdSe reversed type-I core/shell QDs such that the electron wave function distributes largely in the shell region of the small-bandgap CdSe part. This facilitates injection of electrons from the QDs to the TiO_2 substrate, resulting in significantly improved electron-injection efficiency. The enhanced electron-injection efficiency of CdS/CdSe QDs was further confirmed by fluorescence lifetime decay measurements which showed the largest lifetime reduction after the QDs were adsorbed on the TiO_2 surface. The reversed type-I CdS/CdSe QDs showed a higher photon-to-current conversion efficiency (25.2%) than type-I CdSe/CdS (11.3%) and CdSe QDs without shell (17.5%). Furthermore, by forming a quantum-well structure by CBD growth of CdS on the QD-sensitized electrode, the electron-injection efficiency was further enhanced by reducing the electron recombination between the QDs and the redox couple. The absorbed-photon-to-current efficiency of the quantum well CdS/CdSe/CdS sensitized solar cells reaches a value as high as 60%. The results obtained indicate a novel opportunity to improve the photovoltaic performance of nanocrystals by means of sophisticated structural design.

Acknowledgment. This work was partially supported by the Swedish Energy Agency (Contract 32076-1). Z.N. acknowledges the support from Wenner Gren scholarship. We thank Prof. Prashant V. Kamat in Notre Dame Radiation Laboratory for his invaluable advice on fabricating QDSCs and Dr. Heike Hevekerl in Experimental Biomolecular Physics, Royal Institute of Technology, for her assistance in examining optical spectra of the QDs. Mr. Chunze Yuan and Ms. Lin Li are appreciated for their help on the solar-cell performance test.

Supporting Information Available: HRTEM figures of **CdSe-2** and **CdSe/CdS-1** QDs, absorbance, IPCE, and APCE spectra of **CdSe-1**, **CdS/CdSe-1**, and **CdSe/CdS-1** QDs, IPCE spectrum of CdS-sensitized solar cells by CBD adsorption, fluorescence lifetime spectra of **CdS/CdSe-1**, **CdSe/CdS-1**, and **CdSe-2**, and QDs synthesis details. This information is available free of charge via the Internet at http://pubs.acs.org.

References and Notes

(1) (a) Bruchez, M., Jr.; Moronne, M.; Gin, P.; Weiss, S.; Alivisatos, P. *Science* **1998**, *281*, 2013. (b) Narayanan, S. S.; Sinha, S. S.; Verma, P. K.; Pal, S. K. *Chem. Phys. Lett.* **2008**, *463*, 160.

(2) (a) Yong, K.; Roy, I.; Swihart, M. T.; Prasad, P. N. *J. Mater. Chem.* **2009**, *19*, 4655–4672. (b) Molnár, M.; Fu, Y.; Friberg, P.; Chen, Y. *J. Nanobiotechno.* **2010**, *8*, 2. (c) Fu, Y.; Han, T.-T.; Ågren, H.; Lin, L.; Chen, P.; Liu, Y.; Tang, G.-O.; Wu, J.; Yue, Y.; Dai, N. *Appl. Phys. Lett.* **2007**, *90*, 173102. (3).

(3) (a) Huynh, W. U.; Dittmer, J. J.; Alivisatos, A. P. *Science.* **2002**, *295*, 2425. (b) Gur, I.; Fromer, N. A.; Geier, M. L.; Alivisatos, A. P. *Science.* **2005**, *310*, 462. (c) Xu, J.; Wang, J.; Mitchell, M.; Mukherjee, P.; Jeffries-EL, M.; Petrich, J. W.; Lin, Z. *J. Am. Chem. Soc.* **2007**, *129*, 12828–12833. (d) Kim, S.; Kim, W.; Cartwright, A. N.; Prasad, P. N. *Appl. Phys. Lett.* **2008**, *92*, 191107.

(4) (a) Kamat, P. V. *J. Phys. Chem. C* **2007**, *111*, 2834–2860. (b) Kamat, P. V. *J. Phys. Chem. C* **2008**, *112*, 18737–18753. (c) Nozik, A J. *Physica E* **2002**, *14*, 115–120. (d) Li, Y. and ; Zhang, J. Z. *Laser & Photon. Rev.* **2009**, DOI 10.1002/lpor.200910025. . (e) Jin, S.; Lian, T. *Nano, Lett.* **2009**, *9*, 2448–2454. (f) Baruah, S.; Sinha, S. S.; Ghosh, B.; Pal, S. K.; Raychaudhuri, A. K.; Dutta, J. *J. Appl. Phys.* **2009**, *105*, 074308.

(5) Anikeeva, P. O.; Halpert, J. E.; Bawendi, M. G.; Bulović, V. *Nano Lett.* **2009**, *9*, 2532.

(6) For example, (a) Vogel, R.; Hoyer, P.; Weller, H. *J. Phys. Chem.* **1994**, *98*, 3183. (b) Peter, L. M.; Riley, D. J.; Tull, E. J. Wijayantha, K. G. U. *Chem. Commun.* **2002**, *1030*. (c) Lee, Y.; Lo, Y. *Adv. Funct. Mater.* **2009**, *19*, 604–609. (d) Baker, D. R.; Kamat, P. V. *Adv. Funct. Mater.* **2009**, *19*, 805–811. (e) Wang, G.; Yang, X.; Qian, F.; Zhang, J. Z. and Li, Y. *Nano Lett.* **2010**,DOI: 10.1021/nl100250z. (f) Shalom, M.; Dor, S.; Rühle, S.; Grinis, L.; Zaban, Arie *J. Phys. Chem. C* **2009**, *113*, 3895–3898. (g) Sun, W.; Yu, Y.; Pan, H.; Gao, X.; Chen, Q.; Peng, L. *J. Am. Chem. Soc.* **2008**, *130*, 1124–1125. (h) Lin, S.; Lee, Y.; Chang, C.; Shen, Y.; Yang, Y. *Appl. Phys. Lett.* **2007**, *90*, 143517.

(7) For example, (a) Kongkanand, A.; Tvrdy, K.; Takechi, K.; Kuno, M. and; Kamat, P. V. *J. Am. Chem. Soc.* **2008**, *130*, 4007. (b) Liu, D.; Kamat, P. V. *J. Phys. Chem.* **1993**, *97*, 10769. (c) Lee, Y.; Huang, B.; Chien, H. *Chem. Mater.* **2008**, *20*, 6903–6905. (d) Giménez1, S.; Mora-Seró1, I.; Macor, L.; Guijarro, N.; Lana-Villarreal, T.; Gómez, R.; Diguna, L. J.; Shen, Q.; Toyoda, T.; Bisquert, J. *Nanotechnology.* **2009**, *20*, 295204. (e) Shalom, M.; Rühle, S.; Hod, I.; Yahav, S.; Zaban, A. *J. Am. Chem. Soc.* **2009**, *131*, 9876–9877. (f) Hensel, J.; Wang, G.; Li, Y.; Jin, Z. *Nano Lett.* **2010**, *10*, 478–483. (g) Leschkies, K. S.; Divakar, R.; Basu, J.; Enache-Pommer, E.; Boercker, J. E.; Carter, C. B.; Kortshagen, U. R.; Norris, D. J.; Aydil, E. S. *Nano Lett.* **2010**, *7*, 1793–1798.

(8) (a) Plass, R.; Pelet, S.; Krueger, J.; Grätzel, M.; Bach, U. *J. Phys. Chem. B.* **2002**, *106*, 7578. (b) Lee, H.; Leventis, H. C.; Chen, S.; Moon, P.; Ito, S.; Haque, S. A.; Torres, T.; Nüesch, F.; Geiger, T.; Zakeeruddin, S. M.; Grätzel, M.; Nazeeruddin, Md. K. *Adv. Funct. Mater.* **2009**, *19*, 2735–2742. (c) Leventis H, C.; O'Mahony, F.; Akhtar, J.; Afzaal, M.; O'Brien, P.; Haque, S. A. *J. Am. Chem. Soc.* **2010**, *132*, 2743–2750. (d) Hyun, B.-R.; Zhong, Y.; Bartnik, A. C.; Sun, L.; Abruña, H. D.; Wise, F. W.; Goodreau, J. D.; Matthews, J. R.; Leslie, T. M.; Borrelli, N. F. *ACS Nano* **2010**, *2*, 2206.

(9) Yu, P.; Zhu, K.; Norman, A. G.; Ferrere, S.; Frank, A. J.; Nozik, A. J. *J. Phys. Chem. B* **2006**, *110*, 25451.

(10) Peter, L. M.; Wijayantha, K. G. U.; Riley, D. J.; Waggett, J. P. *J. Phys. Chem. B* **2003**, *107*, 8378–8381.

(11) (a) Bang, J. H.; Kamat, P. V. *ACS Nano* **2009**, *3*, 1467. (b) Lee, H.; Wang, M.; Chen, P.; Gamelin, D. R; Zakeeruddin, S. M.; Grätzel, M.; Nazeeruddin, Md. K. *Nano Lett.* **2009**, *9*, 4221–4227.

(12) (a) Luther, J. M.; Law, M.; Beard, M. C.; Song, Q.; Reese, M. O.; Ellingson, R. J.; Nozik, A. J. *Nano Lett.* **2008**, *8*, 3488–3492. (b) Law, M.; Beard, M. C.; Choi, S.; Luther, J. M.; Hanna, M. C.; Nozik, A. J. *Nano Lett.* **2008**, *8*, 3904. (c) Koleilat, G. I.; Levina, L.; Shukla, H.; Myrskog, S. H.; Hinds, S.; Pattantyus-Abraham, A. G.; Sargent, E. H. *ACS Nano* **2008**, *2*, 833. (d) Istrate, E.; Hoogland, S.; Sukhovatkin, V.; Levina, L.; Myrskog, S.; Smith, P. W. E.; Sargent, E. H. *J. Phys. Chem. B* **2008**, *112*, 2757.

(13) (a) Ginger, D. S.; Greenham, N. C. *Phys. Rev. B* **1999**, *59*, 10622. (b) Zhang, J.; Coombs, N.; Kumacheva, E.; Lin, Y.; Sargent, E. H. *Adv. Mater.* **2003**, *15*, 1756. (c) Bartholomew, G. P.; Heeger, A. J. *Adv. Funct. Mater.* **2005**, *15*, 677. (d) Gur, I.; Fromer, N. A.; Chen, C. P.; Kanaras, A. G.; Alivisatos, A. P. *Nano Lett.* **2007**, *7*, 409. (e) Kim, S.; Kim, W.; Cartwright, A. N.; Prasad, P. N. *Sol. Energy Mater. Sol. Cells* **2009**, *93*, 657–661.

(14) (a) Robel, I.; Subramanian, V.; Kuno, M.; Kamat, P. V. *J. Am. Chem. Soc.* **2006**, *128*, 2385. (b) Zaban, A.; Micici, O. I.; Gregg, B. A.; Nozik, A. J. *Langmuir* **1998**, *14*, 3153. (c) Mora-Seró, I.; Giménez, S.; Fabregat-Santiago, F.; Gómez, R.; Shen, Q.; Toyoda, T.; Bisquert, J. *Acc. Chem. Res.* **2009**, *42*, 1848. (d) Buhbut, S.; Itzhakov, S.; Tauber, E.; Shalom, M.; Hod, I; Geiger, T.; Garini, Y.; Oron, D.; Zaban, A. *ACS Nano* **2010**, *4*, 1293–1298.

(15) (a) Hagfeldt, A.; Grätzel, M. *Chem. Rev.* **1995**, *95*, 49. (b) Ning, Z.; Tian, H. *Chem. Commun.* **2009**, 5483–5495. (c) Tian, H.; Yang, X.; Cong, J.; Chen, R.; Liu, J.; Hao, Y.; Hagfeldt, A. Sun, L. *Chem. Commun.* **2009**, 6288.

(16) (a) King, R. R.; Law, D. C.; Edmondson, K. M.; Fetzer, C. M.; Kinsey, G. S.; Yoon, H.; Sherif, R. A.; Karam, N. H. *Appl. Phys. Lett.* **2007**, *90*, 183516. (b) Yamaguchi, M.; Amano, C. *J. Appl. Phys.* **1985**, *58*, 3601.

(17) (a) Mora-Seró, I.; Giménez, S.; Moehl, T.; Fabregat-Santiago, F.; Lana-Villareal, T.; Gómez, R.; Bisquert1, J. *Nanotechnology* **2008**, *19*, 424007. (b) Hodes, G. *J. Phys. Chem. C* **2008**, *112*, 17778. (c) Dibbell, R. S.; Watson, D. F. *J. Phys. Chem.C* **2009**, *113*, 3139–3149.

(18) (a) Takagahara, T.; Takeda, K. *Phys. Rev. B* **1992**, *46*, 15578–15581. (b) Issac, A.; Jin, S.; Lian, T. *J. Am. Chem. Soc.* **2008**, *130*, 11280–11281.

(19) Dayal, S.; Kopidakis, N.; Olson, D. C.; Ginley, D. S.; Rumbles, G. *Nano Lett.* **2010**, *10*, 239–242.

(20) Makhal, A.; Yan, H.; Lemmens, P.; Pal, S. K. *J. Phys. Chem. C* **2010**, *114*, 627–632.

(21) (a) Schaller, R. D.; Klimov, V. I. *Phys. Rev. Lett.* **2004**, *92*, 186601. (b) Ellingson, R. J.; Beard, M. C.; Johnson, J. C.; Yu, P.; Micic, O. I.; Nozik, A. J.; Shabaev, A.; Efros, A. L. *Nano Lett.* **2005**, *5*, 865–871. (c) Service, R. F. *Science* **2008**, *322*, 1784. (d) Fu, Y.; Zhou, Y.-H.; Su, H.; Boey, F. Y. C., Ågren, H. *J. Phys. Chem. C* **2010**, DOI: 10.1021/jp9082486.

(22) Kim, S.; Fisher, B.; Eisler, H.-J.; Bawendi, M. *J. Am. Chem. Soc.* **2003**, *125*, 11466–11467.

(23) Diguna, L. J.; Shen, Q.; Kobayashi, J.; Toyoda, T. *App. Phys. Lett.* **2007**, *91*, 023116.

(24) (a) Yu, W. W.; Peng, X. *Angew. Chem., Int. Ed.* **2002**, *41*, 2368. (b) Battaglia, D.; Li, J. J.; Wang, Y.; Peng, X. *Angew. Chem., Int. Ed.* **2003**, *42*, 5035–5039. (c) Peng, Z. A.; Peng, X. *J. Am. Chem. Soc.* **2001**, *123*, 183–184.

(25) (a) Nazeeruddin, Md. K.; Kay, A.; Rodicio, I.; Humpbry-Baker, R.; Müller, E.; Liska, P.; Vlachopoulos, N.; Grätzel, M. *J. Am. Chem. Soc.* **1993**, *115*, 6382. (b) Ning, Z.; Zhang, Q.; Wu, W.; Tian, H. *J. Organomet. Chem.* **2009**, *694*, 2705.

(26) Yu, W. W.; Qu, L.; Guo, W.; Peng, X. *Chem. Mater.* **2003**, *15*, 2854–2860.

(27) (a) Embden, J.; Jasieniak, J.; Mulvaney, P. *J. Am. Chem. Soc.* **2009**, *131*, 14299–14309. (b) Xie, R.; Kolb, U.; Li, J.; Basché, T.; Mews, A. *J. Am. Chem. Soc.* **2005**, *127*, 7480–7488.

(28) Madelung, O. *Data in Science and Technology: Semiconductors other than Group IV Elements and III-V Compounds*; Springer: Boston, 1992.

(29) Hussain, O. M.; Rao, K. S.; Madhuri, K. V.; Uthanna, S.; Julien, C. *Electrochem. Soc. Proc.* **2003**, *17*, 56–61.

(30) Fillinger, A.; Parkinson, B. A. *J. Electrochem. Soc.* **1999**, *146*, 4559–4564.

JP102978G